International Journal of Mechanics and Energy (IJME)
Vol. 13, Issue 1, 2026, ISSN: 2286-5845

Numerical investigation of the surface roughness effect on the cavitation dynamics over a NACA66 hydrofoil

Sobhi Frikha*, Mounir Baccar

Advanced Fluid Dynamics, Energetics and Environment, (AFD2E) National Engineering School of Sfax, University of Sfax, B.P. 1173, km 3.5 Soukra, 3038 Sfax, TUNISIA

Abstract: This paper presents a detailed numerical study of cavitating flow over a NACA66 hydrofoil at a cavitation number of 0.99. Validation against experimental data demonstrated accurate prediction of cavity dynamics, lift and drag forces, and shedding frequency. The effects of surface roughness were analyzed, showing performance degradation with increased roughness, where a smooth surface yielded the best hydrodynamic efficiency and stable cavitation behavior. The study underscores the potential of the surface texture as a passive control method to mitigate cavitation-induced instabilities while preserving hydrofoil performance, providing valuable insights for the design of efficient cavitating hydrofoils and propulsors.

Key words: CFD, FLUENT, cavitation, roughness, control.

1. Introduction

Cavitation, a complex and multifaceted phenomenon in fluid mechanics, has been a subject of extensive research due to its significant implications in various engineering applications, including hydraulic turbines, pumps, and marine propellers. The associated instabilities, arising from the nucleation, growth, and violent collapse of vapor bubbles, are known to cause structural erosion, acoustic emissions, and significant losses in hydraulic efficiency. Understanding and controlling these instabilities are crucial for optimizing the performance and longevity of hydraulic machines.

Cavitation instabilities manifest in two primary regimes: an unstable regime characterized by cloud cavitation shedding and a stable regime with a pulsating sheet cavity. The unstable regime is particularly detrimental as it leads to violent bubble collapses, causing erosion and noise. In contrast, the stable regime, though less aggressive, still poses challenges in maintaining consistent system performance. The transition between these regimes is influenced by various factors, including the geometry of the system, operating conditions, and surface roughness [1,2].

Recent studies have shown that cavitation instabilities are not isolated to specific components but can propagate through the system, affecting overall performance. For instance, in hydro turbines, overload surge and surge mode oscillations at part load have been linked to the diffuser effect of the draft tube. These instabilities are further exacerbated by the interaction of the local flow near the cavity trailing edge with the leading edge of the next blade, as observed in turbopump inducers [1, 3, 4].

The study of cavitation instabilities requires a combination of experimental and numerical approaches to capture the complex dynamics of bubble formation and collapse. Experimental techniques such as Laser Doppler Velocimetry, visualizations, and pressure measurements have been instrumental in understanding cavitation behavior in various geometries, including Venturi-type obstacles and hydrofoils [5,6,7].

Complementing experimental studies, numerical methods, particularly Computational Fluid Dynamics (CFD), have emerged as powerful tools for simulating cavitation phenomena. CFD enables detailed analysis

*** Corresponding author:** Sobhi Frikha
E-mail: sobhi.frikha@enis.tn

of flow fields, pressure distributions, and vapor structures under various operating conditions. Both two-dimensional and three-dimensional models have been successfully applied to investigate cavitation instabilities [8,9,10].

Controlling cavitation instabilities is essential to mitigate their adverse effects on hydraulic systems. Passive control methods, which modify surface conditions, have shown strong potential in reducing cavitation intensity [11,12,13]. Among these methods, surface roughness plays a crucial role in determining cavitation behavior. Roughness can alter the flow field by enhancing turbulence and modifying the boundary layer structure. These effects may either suppress or intensify cavitation depending on the roughness characteristics. Studies have demonstrated that structured roughness, such as longitudinal grooves, can reduce sheet cavity length and suppress cloud cavitation shedding. In contrast, random roughness tends to promote more aggressive cavitation due to increased turbulence and pressure fluctuations [14,15,16].

Active control methods, involving real-time adjustments of operating conditions such as pressure and flow rate, can also stabilize cavitation regimes. However, these approaches are often complex and require advanced control systems. Passive strategies based on surface modification remain attractive due to their simplicity, although they must be carefully designed to avoid performance degradation [17,18,19]. Cavitation instabilities remain a critical challenge in hydraulic systems, requiring a comprehensive understanding of their mechanisms. Through a combination of experimental and numerical approaches, this study investigates the effects of surface roughness on cavitation dynamics, providing valuable insights into the control of cavitation instabilities. The findings offer important perspectives for the design and optimization of efficient and durable hydraulic systems.

Nomenclature

σ: Cavitation number (–)
C_μ: k-ε model constant
C_L: Lift coefficient (–)
C_D: Drag coefficient (–)
f: Shedding frequency (Hz)
F_{vap}, F_{cond}: Evaporation and condensation coefficients
G_k, G_b: Turbulence production terms
k: Turbulent kinetic energy (m^2/s^2)
ks: Sand-grain roughness height (μm)
Cs: Roughness constant (–)
L: Cavity length (m)
C: Chord length (m)
n: Bubble number density (m^{-3})
P: Static pressure (Pa)
P_{ref}: Reference outlet pressure (Pa)
P_{vap}: Vapor pressure (Pa)
R_B: Bubble radius (m)
Str: Strouhal number (–)
V_{ref}: Reference inlet velocity (m/s)
V_m: Mass-averaged mixture velocity (m/s)
α_k: Volume fraction of phase k (–)
ε: Turbulent dissipation rate (m^2/s^3)
μ_m: Mixture dynamic viscosity (Pa·s)
μ_t: Turbulent viscosity (Pa·s)
ρ_m, ρ_l, ρ_v: Mixture, liquid, and vapor densities (kg/m^3)

2. Numerical model

2.1 Numerical method

Computational Fluid Dynamics (CFD) simulations were performed using ANSYS Fluent, under turbulent flow conditions. The software employs a finite volume method to discretize and solve the Navier-Stokes equations, allowing for a detailed examination of the flow characteristics. The simulation setup mirrors the experimental configuration of Wang et al. (2020), which features a NACA66 hydrofoil inclined at 8° with a chord length of 0.07 m.

At the inlet, a reference velocity V_{ref} is prescribed, while the outlet is defined by a pressure boundary condition. The outlet pressure P_{ref} is calculated using the cavitation number σ, defined as:

$$\sigma = \frac{P_{ref} - P_{vap}}{\frac{1}{2}\rho V_{ref}^2} \quad (1)$$

where P_{vap} is the vapor pressure of water. This dimensionless parameter serves to evaluate the propensity for cavitation, representing the ratio of the static-to-dynamic pressure difference. It is a key indicator in the analysis of cavitating flows and is essential for the design and reliability of hydraulic systems.

Accordingly, the outlet pressure is determined as:

$$P_{ref} = \sigma.\frac{1}{2}\rho V_{ref}^2 + P_{vap} \quad (2)$$

The boundary conditions and mesh structure of the computational domain are illustrated in Figure 1.

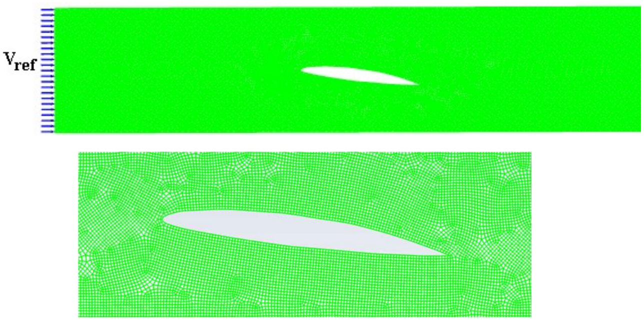

Fig.1 Meshing of the control volume and Boundary conditions

To ensure reproducibility, the thermophysical properties of the working fluid and the operating conditions used in the simulations are explicitly summarized in Table 1. The working fluid is liquid water at a reference temperature of 25°C, with dissolved non-condensable air included as a third phase. Incompressible and isothermal flow is assumed throughout all simulations.

Table 1 Fluid properties and operating conditions

Properties	Values
liquid water density	$\rho_l = 998.2\ kg/m^3$
liquid dynamic viscosity	$\mu_l = 1.003 \times 10^{-3} Pa \cdot s$
water vapor density	$\rho_v = 0.5542\ kg/m^3$
vapor dynamic viscosity	$\mu_v = 9.8 \times 10^{-6} Pa \cdot s$
reference temperature	T = 25°C

2.2. Mathematical formulation

The flow exhibits multiphasic behavior comprising three distinct phases: liquid water, vapor, and air. In our study, we have employed the mixture model to simulate this complex interaction.

Continuity equation:

The continuity equation governing the mixture flow is expressed as:

$$\frac{\partial}{\partial t}(\rho_m) + \nabla.(\rho_m \vec{V}_m) = 0 \quad (3)$$

Where $\vec{V}_m$ is the mass-averaged velocity:

$$\vec{V}_m = \frac{\sum_{k=1}^{n} \alpha_k \vec{V}_k}{\rho_m} \quad (4)$$

Here ρ_m denotes the mixture density:

$$\rho_m = \sum_{k=1}^{n} \alpha_k \rho_k \quad (5)$$

α_k is the volume fraction of phase k.

Momentum equation:

The momentum equation for the mixture is derived by summing the momentum equations for all individual phases and is expressed as:

$$\frac{\partial}{\partial t}(\rho_m \vec{V}_m) + \nabla.(\rho_m \vec{V}_m \vec{V}_m) = -\nabla p + \nabla.\left[\mu_m(\nabla \vec{V}_m + \nabla \vec{V}_m^T)\right] + \rho_m \vec{g} + \vec{F} - \nabla.\left(\sum_{k=1}^{n} \alpha_k \rho_k \vec{V}_{dr,k} \vec{V}_{dr,k}\right) \quad (6)$$

Here n is the number of phases, $\vec{F}$ is a body force, and μ_m is the viscosity of the mixture :

$$\mu_m = \sum_{k=1}^{n} \alpha_k \mu_k \quad (7)$$

Turbulence model

A modified k-ε RNG turbulence model is employed in this study. The turbulent viscosity is expressed as:

$$\mu t = f(\rho)\, C\mu \frac{k^2}{\varepsilon} \quad (8)$$

Where

$$f(\rho) = \rho_v + (1 - \alpha)^n (\rho_l - \rho_v) \quad (9)$$

n is set to the value of 10, as recommended by Coutier-Delgosha et al. in 2003.

The transport equations for the k-ε RNG model are given by:

$$\frac{\partial}{\partial t}(\rho k) + \frac{\partial}{\partial x_i}(\rho k\, u_i) = \frac{\partial}{\partial x_i}\left(\alpha_k \mu_{eff} \frac{\partial k}{\partial x_j}\right) + G_k + G_b - \rho\epsilon - Y_M + S_k \quad (10)$$

$$\frac{\partial}{\partial t}(\rho\epsilon) + \frac{\partial}{\partial x_i}(\rho\epsilon\, u_i) = \frac{\partial}{\partial x_i}\left(\alpha_\epsilon \mu_{eff} \frac{\partial \epsilon}{\partial x_j}\right) + G_{1\epsilon}\frac{\epsilon}{k}(G_k + C_{3G}G_b) - C_{2\epsilon}\rho\frac{\epsilon^2}{k} - R_\epsilon + S_\epsilon \quad (11)$$

In these equations:

- G_k is the production of turbulence kinetic energy due to the velocity gradients.
- G_b is the production of turbulence kinetic energy due to buoyancy.
- Y_M accounts for the effect of fluctuating dilatation in compressible turbulence on the dissipation rate
- α_k and α_ϵ are the inverse effective Prandtl numbers for k and ϵ, respectively.
- S_k and S_ϵ are user-defined source terms.

In our study, we implemented a User Defined Function (UDF) in ANSYS Fluent to incorporate the modified k-epsilon RNG turbulence model expression into the simulation.

Cavitation model

The equation for the vapor volume fraction has the general form:

$$\frac{\partial}{\partial t}(\alpha\rho_V) + \nabla.\left(\alpha\rho_V\vec{V}\right) = R_e + R_C \quad (12)$$

In ANSYS Fluent, two widely used cavitation models are available: the Schnerr–Sauer model and the Zwart–Gerber–Belamri (ZGB) model. In this study, we adopted the Schnerr–Sauer model, which is defined as follows:

When $P_V \geq P$,

$$R_e = F_{vap}\frac{\rho_V\rho_l}{\rho}\alpha(1-\alpha)\frac{3}{R_B}\sqrt{\frac{2}{3}\frac{(P_V - P)}{\rho_l}} \quad (13)$$

When $P_V \leq P$,

$$R_c = F_{cond}\frac{\rho_V\rho_l}{\rho}\alpha(1-\alpha)\frac{3}{R_B}\sqrt{\frac{2}{3}\frac{(P_V - P)}{\rho_l}} \quad (14)$$

F_{vap} et F_{cond} are the empirical calibration coefficients of evaporation and condensation with the default value of 1 and 0.2, respectively.

R_B is the bubble radius, it is defined by:

$$R_B = \left(\frac{\alpha}{1-\alpha}\frac{3}{4\pi}\frac{1}{n}\right)^{\frac{1}{3}} \quad (15)$$

n is the number of bubbles per volume of liquid.

3. Numerical results

To assess the reliability of the numerical predictions, a grid independence study was carried out using three successively refined mesh levels: coarse (approximately 40,000 cells), medium (approximately 80,000 cells), and fine (approximately 160,000 cells). The monitored quantities included the time-averaged lift coefficient CL, the cavity length ratio L/C, and the shedding frequency f. Differences between the medium and fine meshes were below 1% for all quantities; consequently, the medium mesh was retained for all subsequent simulations as the best compromise between accuracy and computational cost. Regarding temporal resolution, a time-step sensitivity study confirmed that a dimensionless time step of Δt·Vref/C = 5 × 10⁻4 ensures time-step-independent results, with relative differences in shedding frequency below 0.5% compared to a two-fold finer time step. Convergence was monitored at each time step, with scaled residuals required to drop below 10⁻5 for continuity and momentum equations before advancing to the next step.

3.1. Evolution of cavitation dynamics

This study presents numerical simulations of flow over a NACA66 hydrofoil at a cavitation number of 0.99. The cavitating flow was modeled using the Schnerr and Sauer approach, which effectively captures the phase change dynamics involved.

The primary objective was to compare the development of the cavitation sheet along the suction side of the hydrofoil against the experimental results published by Wang et al. [28]. Rather than forming a stable cavitation sheet, the simulations revealed the emergence of an unsteady cavitation cloud, exhibiting noticeable variations in size, shape, and position over time, hallmarks of transient cavitation behavior (see Fig. 2).

These unsteady characteristics are in strong agreement with experimental findings available in the literature, lending further credibility to the numerical framework employed in this investigation.

The observed cavity dynamics are largely attributed to the action of a re-entrant jet, which flows upstream along the foil's surface within the boundary layer. This jet induces hydrodynamic instabilities, ultimately triggering the periodic shedding of vapor structures, forming discrete vapor clouds.

The results provide key insights into the hydrodynamic and cavitation behavior of the NACA66 foil. A lift-to-drag ratio (C_L/C_D) of 5.838 indicates efficient performance, with a high lift relative to drag. The lift force and drag force, used to calculate this ratio, are obtained from the numerical data shown in Figure 3 and Figure 4, respectively. The cavity length ratio (L/C) derived from simulations is 0.689, which closely matches the experimental value of 0.700, confirming the validity and accuracy of the numerical model in capturing steady cavitation characteristics. The shedding frequency (f) of 17.4 Hz is determined based on the time evolution of the lift force, capturing the unsteady behavior of the cavitating flow. (Fig 5) The corresponding Strouhal number is Str = 0.107.

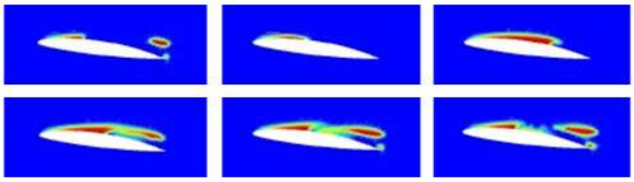

(a) Numerical simulation with Schnerr and Sauer Model

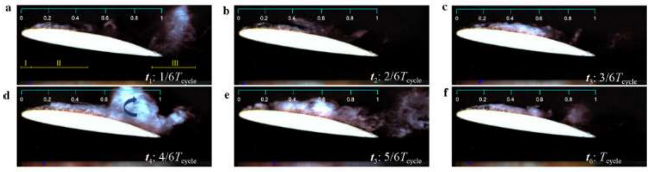

(b) Experimental data of Wang et al. [28]

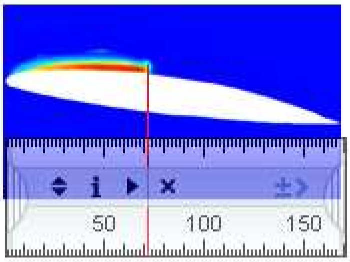

(c) Measurement of the maximal length of the attached cavity

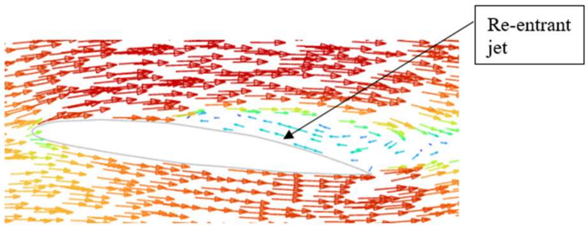

(d) Velocity vector field highlighting the presence of a re-entrant jet

Fig.2 Temporal evolution of partial cavities, σ = 0.99, C = 0.07 m, the time instants shown correspond to one shedding cycle of period T = 1/f ≈ 0.057 s.

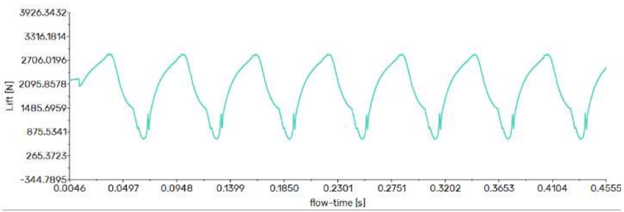

Fig 3 Time evolution of the lift force

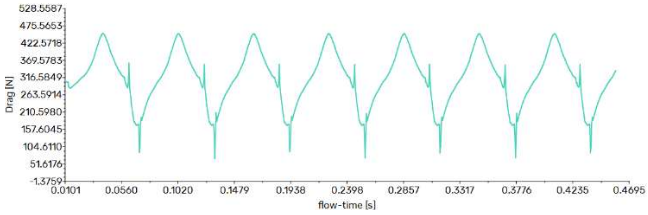

Fig 4 Time evolution of the drag force

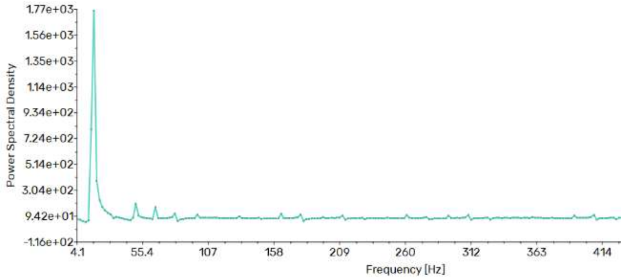

Fig 5 Power spectral density of the lift force signal; the dominant peak at 17.4 Hz corresponds to the cavity shedding frequency (Str = 0.107)

3.2. Influence of surface roughness on cavitation dynamics

In ANSYS Fluent, wall roughness is modeled by specifying parameters such as the roughness height (k_s) and the roughness constant (C_s) at the wall boundary conditions. These parameters account for the effects of surface irregularities on turbulent flow and heat transfer, especially within the near-wall region. Fluent uses a sand-grain roughness model, where the roughness height represents the size of the roughness elements and modifies the logarithmic velocity profile in the turbulent boundary layer.

Roughness Height (k_s): This is the primary input and represents the equivalent sand-grain roughness height. A value of zero corresponds to a hydraulically smooth wall. In our simulations, the values reported in Table 2 directly correspond to the k_s values specified in Fluent. These were chosen to match the physical roughness elements used in the experimental tests for consistency and validation purposes.

Roughness Constant (C_s): This parameter relates to the shape and distribution of the roughness elements. In our case, we used the default Fluent value of $C_s = 0.5$, which is appropriate for uniform sand-grain-type roughness. Values between 0.5 and 1 are typical for engineering surfaces.

Fluent incorporates these parameters into the modified wall-function formulation. The wall shear stress and velocity profile are adjusted using the roughness function.

While this method is an engineering approximation, primarily developed for fully turbulent, attached boundary layers, recent research has demonstrated its relevance and effectiveness even in complex flow conditions involving cavitation and flow separation. For instance, Samadi-Boroujeni et al. [20] validated roughness-based simulations of chute spillways against measured cavitation indices, showing that the model could reliably capture the effect of roughness on cavitation inception. Similarly, Al Bishtawi et al. [21,22] applied rough-wall models to centrifugal pumps and reported that increased blade roughness modified both the pressure field and cavitation behavior, including delayed inception and shifted cavity location, with trends consistent with physical expectations. These findings support the applicability of wall-function-based roughness modeling to a broader class of separated and cavitating flows.

In our simulations, roughness was applied uniformly on the suction side of the airfoil surface, particularly in the region susceptible to cavitation and boundary layer separation, based on experimental observations. The pressure side of the airfoil was kept hydraulically smooth in all cases. This selective application allowed us to isolate and investigate the effects of suction-side roughness on flow behavior and cavitation control.

The table 2 presents the influence of surface roughness on the hydrodynamic performance and cavitation behavior, detailing the roughness levels along with the corresponding lift-to-drag ratio (C_L/C_D), normalized cavity length (L/C), shedding frequency (f), and Strouhal number (Str).

Figures 6, 7, and 8 show the evolution of maximum cavity length (L_{max}/C), Strouhal number, and lift-to-drag ratio (C_L/C_D), respectively, as functions of surface roughness.

Table 2 Roughness effect on cavitation

Roughness	C_L/C_D	L/C	f	Str
0	5,838	0,689	17,400	0,107
100	5,790	0,614	16,2	0,089
200	5,590	0,582	16,700	0,087
400	5,440	0,571	16,800	0,086
1000	5,274	0,566	16,1	0,081

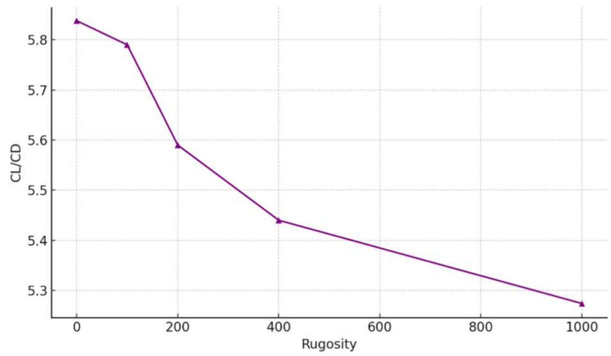

Fig 6 Evolution of lift-to-drag ratio (C_L/C_D), as functions of surface roughness

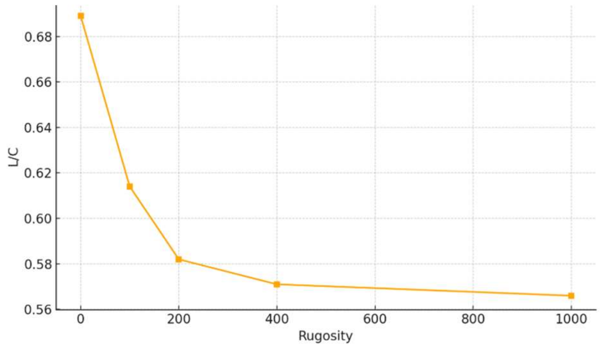

Fig 7 Evolution of maximum cavity length (L_{max}/C), as functions of surface roughness

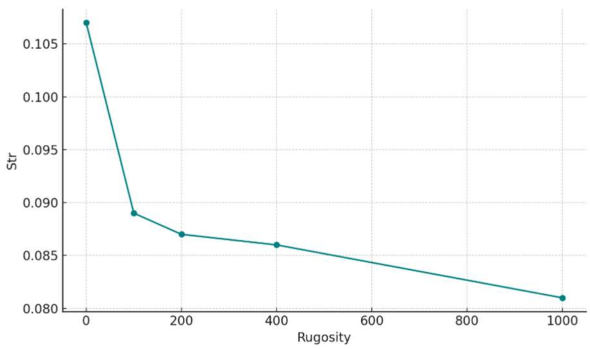

Fig 8 evolution of Strouhal number as functions of surface roughness

The effect of surface roughness on hydrodynamic or aerodynamic performance is evident through the progressive changes observed in the lift-to-drag ratio (C_L/C_D), the relative cavitation length (L/C), and the Strouhal number (Str). For a smooth surface (roughness = 0), the system operates at its peak efficiency, with a C_L/C_D of 5.838, indicating an optimal balance between lift and drag. The cavitation length ratio (L/C) is also at its highest, 0.689, meaning the low-pressure cavity extends further along the chord. Simultaneously, the Strouhal number is 0.107, which reflects a moderate level of flow oscillations typically associated with stable vortex shedding from the cavitating region.

As surface roughness increases to 100, the C_L/C_D drops slightly to 5.79, signaling a small loss in aerodynamic performance due to added skin friction and turbulent effects. The L/C also decreases to 0.614, indicating a shorter cavity length, possibly because the rough surface disrupts the pressure gradient necessary to sustain a longer cavitation zone. The Strouhal number drops significantly to 0.089, suggesting a reduction in the frequency or amplitude of oscillations in the cavitating flow. This trend continues with increasing roughness. At roughness = 200, C_L/C_D falls to 5.59, and L/C drops to 0.582. The Strouhal number also slightly decreases to 0.087, showing that the flow becomes marginally more stable or less prone to high-frequency fluctuations.

With even rougher surfaces, such as roughness = 400, the negative impact on performance becomes more pronounced.C_L/C_D reduces further to 5.44, and L/C continues its downward trend to 0.571. The Strouhal number decreases only marginally to 0.086, indicating a stabilization of the flow, though not necessarily beneficial, as it comes with a performance cost. Finally, at roughness = 1000, the surface is significantly roughened, and the aerodynamic efficiency is at its lowest, with C_L/C_D = 5.274, representing a substantial decrease from the smooth case. The cavitation length ratio is also at its minimum, 0.566, and Str drops to 0.081, the lowest value in the dataset, indicating the least unsteady behavior of the cavity.

In summary, increasing roughness consistently degrades aerodynamic efficiency (C_L/C_D) due to the higher skin friction and premature flow transition or separation induced by surface irregularities. The shortening of the cavitation zone (lower L/C) suggests that roughness limits the development or sustainment of low-pressure regions, which could either delay cavitation inception or suppress its extent. Meanwhile, the decreasing Strouhal number reflects a reduction in the unsteadiness of the cavitating flow, possibly due to a more diffuse and less energetic vortex shedding process. While this might seem beneficial for flow stability, it is accompanied by a clear loss in performance. Thus, for applications where high lift, low drag, and controlled cavitation are essential, maintaining a smooth surface is critical. Even moderate levels of surface roughness result in measurable and consistent performance deterioration.

4.Conclusion

This study presented a comprehensive numerical investigation of cavitating flow over a NACA66 hydrofoil using the Schnerr and Sauer cavitation model at a cavitation number of 0.99. The simulation results were validated against experimental data from Wang et al. [28], showing strong agreement in terms of cavity dynamics and cavity length. The model successfully reproduced key features of cloud cavitation, particularly the formation of unsteady vapor structures induced by a re-entrant jet mechanism.

In addition to model validation, the influence of surface roughness on cavitation behavior and hydrodynamic performance was systematically analyzed. The results demonstrated a clear degradation of performance with increasing roughness. While low to moderate roughness levels (e.g., 100–200 μm) led to a slight reduction in cavity length and unsteadiness, higher roughness values consistently resulted in lower lift-to-drag ratios and shorter cavities. Moreover, reduced Strouhal numbers indicated a damping of periodic shedding activity.

The smooth surface configuration (roughness = 0) was identified as the optimal case, providing the highest hydrodynamic efficiency with CL/CD=5.838, a cavity length ratio of L/C=0.689, and a Strouhal number of Str=0.107. These results reflect a balance between aerodynamic performance and controlled cavitation dynamics.

Overall, the findings highlight the significant role of surface roughness as a passive control parameter influencing cavitation behavior. Proper surface finishing can contribute to mitigating cavitation-induced instabilities while preserving hydrodynamic efficiency. These results provide valuable insights for the design and optimization of hydrofoils and propulsors operating under cavitating conditions, emphasizing the importance of surface treatment in achieving stable and efficient performance.

References

[1] Tsujimoto, Y. (2013, December). Cavitation instabilities in hydraulic machines. In IOP Conference Series: Materials Science and Engineering (Vol. 52, No. 1, p. 012005). IOP Publishing.

[2] Danlos, A., Méhal, J. E., Ravelet, F., Coutier-Delgosha, O., & Bakir, F. (2014). Study of the cavitating instability on a grooved Venturi profile. Journal of Fluids Engineering, 136(10), 101302.

[3] Matsuzaka, R., Nakashima, T., & Miyagawa, K. (2016, November). Study on flow instability in a diffuser with swirling flow under several conditions of pipe length and swirl intensity. In IOP Conference Series: Earth and Environmental Science (Vol. 49, No. 8, p. 082015). IOP Publishing.

[4] Luo, X. W., Ji, B., & Tsujimoto, Y. (2016). A review of cavitation in hydraulic machinery. Journal of Hydrodynamics, 28(3), 335-358.

[5] Yin, J., Zhang, Y., Gong, D., Tian, L., & Du, X. (2023). Dynamics of a laser-induced cavitation bubble near a cone: an experimental and numerical study. Fluids, 8(8), 220.

[6] Hitt, M., Lineberry, D., Ahuja, V., & Frederick, R. (2012, July). Experimental investigation of cavitation induced feedline instability from an orifice. In 48th AIAA/ASME/SAE/ASEE Joint Propulsion Conference & Exhibit (p. 4029).

[7] Wang, H., Feng, J., Liu, K., Shen, X., Xu, B., Zhang, D., & Zhang, W. (2022). Experimental study on unsteady cavitating flow and its instability in liquid rocket engine inducer. Journal of Marine Science and Engineering, 10(6), 806.

[8] Frikha, S., Coutier-Delgosha, O., & Astolfi, J. A. (2008). Influence of the cavitation model on the simulation of cloud cavitation on 2D foil section. International Journal of Rotating Machinery, 2008(1), 146234.

[9] Nakashima, T., Enomoto, Y., & Nakamura, T. (2024, February). Numerical analysis of flow instability with vortex cavitation in venturi tube. In Journal of Physics: Conference Series (Vol. 2707, No. 1, p. 012146). IOP Publishing.

[10] Wang, Y. (2023, August). On suitable CFD setups for cavitation dynamics. In IOP Conference Series: Materials Science and Engineering (Vol. 1288, No. 1, p. 012053). IOP Publishing.

[11] Zaresharif, M., Ravelet, F., Kinahan, D. J., & Delaure, Y. (2021). Cavitation control using passive flow control techniques. Physics of Fluids, 33(12).

[12] Capurso, T., Lorusso, M., Camporeale, S. M., Fortunato, B., & Torresi, M. (2019, March). Implementation of a passive control system for limiting cavitation around hydrofoils. In IOP Conference Series: Earth and Environmental Science (Vol. 240, No. 3, p. 032025). IOP Publishing.

[13] Kadivar, E., & el Moctar, O. (2019, March). Boundary layer instability control in the unsteady cloud cavitating flow. In IOP Conference Series: Earth and Environmental Science (Vol. 240, No. 6, p. 062061). IOP Publishing.

[14] Coutier-Delgosha, O., Devillers, J., Leriche, M., and Pichon, T. (April 1, 2005). "Effect of Wall Roughness on the Dynamics of Unsteady Cavitation." ASME. J. Fluids Eng. July 2005; 127(4): 726–733. https://doi.org/10.1115/1.1949637

[15] Hao, J., Zhang, M., & Huang, X. (2018). The influence of surface roughness on cloud cavitation flow around hydrofoils. Acta Mechanica Sinica, 34, 10-21.

[16] Stutz, B. (2003). Influence of roughness on the two-phase flow structure of sheet cavitation. J. Fluids Eng., 125(4), 652-659.

[17] Mongeau, L., Kook, H., & Franchek, M. (1998, January). Active control of flow-induced cavity resonance. In 4th AIAA/CEAS Aeroacoustics Conference (p. 2349).

[18] Aradag, S., Gelisli, K. A., & Yaldir, E. C. (2017). Effects of active and passive control techniques on Mach 1.5 cavity flow dynamics. International Journal of Aerospace Engineering, 2017(1), 8253264.

[19] Yin, Y. (2023). Current study on active flow control and passive flow control. Theoretical and Natural Science, 26, 227-234.

[20] Samadi-Boroujeni, H., Abbasi, S., Altaee, A., & Fattahi-Nafchi, R. (2020). Numerical and physical modeling of the effect of roughness height on cavitation index in chute spillways. International Journal of Civil Engineering, 18(5), 539-550.

[21] Al Bishtawi, B., Scribano, G., & Tran, M. V. (2022). Numerical analysis on the effect of blade roughness on cavitating flow characteristics in centrifugal pumps. Journal of the Brazilian Society of Mechanical Sciences and Engineering, 44(7), 305.

[22] Al Bishtawi, B., Scribano, G., & Tran, M. V. (2021, October). Numerical study of blade roughness effect on cavitation in centrifugal pumps. In Journal of Physics: Conference Series (Vol. 2051, No. 1, p. 012047). IOP Publishing